AIMS Energy, 13(2): 231–247.
DOI: 10.3934/energy.2025008
Received: 28 October 2024
Revised: 31 January 2025
Accepted: 25 February 2025
Published: 04 March 2025

https://www.aimspress.com/journal/energy

Research article

Self-draining bipolar plate: Experimentation with various catalyst-loading in a low temperature proton exchange membrane fuel cell

Sudesh Bekal[1,2,*] and Shripad T Revankar[3]

[1] NMAM Institute of Technology, Nitte-574110, KA, India
[2] NITTE Deemed to be University, Mangaluru, KA, India
[3] School of Nuclear Engineering, Purdue University, West Lafayette, IN 47907 USA

*** Correspondence:** Email: sudeshbekal@nitte.edu.in; Tel: +8904010966.

Abstract: The paper presents the results of experimental studies on a self-draining bipolar plate used in a low-temperature polymer electrolyte membrane fuel cell (L-PEMFC). These studies investigated the cell's performance under varying platinum catalyst loadings and different hydrogen and oxygen flow rates.

Two catalyst loading configurations were tested: (i) 0.20 mg/cm^2 (anode) and 0.40 mg/cm^2 (cathode) and (ii) 0.25 mg/cm^2 (anode) and 0.50 mg/cm^2 (cathode). The gas diffusion layer (GDL) employed was carbon paper, with the catalyst arranged on the carbon substrate.

Hydrogen flow rates of 80, 100, and 120 ml/min were assessed alongside oxygen supplies at 50%, 100%, and 150% excess relative to the stoichiometric requirement (0%) in relation to the hydrogen supply for both catalyst loading conditions. Additional experiments were conducted at humidification temperatures of 60, 70, 80, 90, and 100 ℃, using the optimal hydrogen flow rate and oxygen supply conditions. To evaluate the stability, the fuel cell operated continuously for 5 hours at the optimal humidification temperature to assess the stability of voltage and power output.

The fuel cell using the self-draining bipolar plate demonstrated an approximately 30% increase in load-bearing capacity. However, it did not show significant differences in voltage or power across the varying catalyst loadings. The optimal humidification temperature was determined to be 90 ℃. This study provides valuable insights into the continuous operation of fuel cells under optimal conditions of humidification, excess oxygen, and hydrogen flow rate.

Keywords: self-draining plate; voltage over-potential; continuous operation; humidification temperature; maximum power point

1. Introduction

Among the various types of fuel cells, polymer electrolyte membrane (PEM) fuel cells are particularly promising for automotive applications due to their high energy density at low operating temperatures, rapid start-up capabilities, zero emissions, and overall system robustness [1–3]. However, several operational challenges must be addressed for their practical implementation, including the high costs of the membrane and catalyst, inefficient gas distribution across the membrane electrode assembly (MEA), and excess moisture at both the anode and cathode. This paper focuses on improving hydrogen gas distribution and reducing moisture on the anode side of the fuel cell.

In a fuel cell, the anode not only receives water from the hydrogen feed but also experiences water influx from the cathode through back diffusion. Flooding in conventional serpentine channels impairs hydrogen gas distribution across the MEA and can ultimately halt gas flow, leading to operational failure. Additionally, conventional serpentine channels often suffer from significant concentration losses in the later stages of flow, which exacerbates the performance issues.

Water flooding in proton exchange membrane fuel cells (PEMFCs) poses a significant challenge that affects both performance and durability. Flooding can lead to performance degradation by obstructing the supply of reactants and can also introduce safety risks, such as cell reversal [4]. Research suggests that employing suitable flow field structures, optimizing the operating conditions, and utilizing porous inserts can help alleviate flooding issues and improve water management in PEMFCs [5–8].

Experimental studies have shown that specific flow field designs, such as double serpentine structures, along with optimal relative humidity conditions, can enhance water management and increase power density [5,6]. Additionally, multiphase, non-isothermal physics-based models have been developed to estimate cells' performance under flooding conditions, providing insights into reactant transport and membrane water content [7]. Recent research has also focused on creating systems that employ deep learning and image processing techniques to diagnose and detect flooding and drying in PEMFCs, aiming to maintain normal operation and enhance stability [9,10]. Operating parameters such as flow rates, pressure, and relative humidity significantly influence the presence of liquid water in flow channels, thereby affecting fuel cells' performance [11,12]. Effective water management is crucial for ensuring optimal performance and durability in proton exchange membrane fuel cells (PEMFCs). The accumulation of liquid water at the gas diffusion layer can obstruct reactant gas pathways, inhibiting electrochemical reactions [13]. Dynamic modeling and control strategies, such as active disturbance rejection control (ADRC) and closed-loop management systems, have been proposed to enhance water management and improve energy efficiency [14,15]. Experimental approaches, including internal dehumidification and the use of capillary arrays, have been explored to mitigate water flooding and improve the stack's voltage and temperature distribution [16,17]. A stepped flow field enhances the distribution of gas concentration, velocity, and current density, resulting in a 21.5% increase in net power compared with traditional parallel flow fields [18]. The in-plane design of the gas diffusion layer (GDL), which incorporates high water

retention capabilities near the reactant gas inlet and enhanced gas diffusion near the outlet, significantly improves performance, achieving up to 75% better uniformity in the current distribution [19]. Large eddy simulations indicate that Z-type inlet-outlet configurations provide a more uniform flow distribution and fewer fluctuations compared with U-type configurations, offering valuable guidance for header design [20].

A self-draining system was designed to mitigate flooding in proton exchange membrane fuel cells (PEMFCs). The gravitational force acting on the droplets facilitates their removal, creating space for gas flow [21] resulting in improved efficiency and stability [22].

This work extends previous research aimed at addressing flooding in PEMFCs. It involves the development of a specialized bipolar plate that features a chamber and a draining plate with multiple conical passageways. These passage ways guide the gases entering the chamber towards the MEA of the fuel cell and facilitate self-draining of the liquid through gravity and eddies. The objective of the study was to evaluate whether reducing the platinum catalyst concentration influences the fuel cell's performance under varying hydrogen flow rates and excess oxygen supplies, as well as to determine the optimal humidification temperature for hydrogen gas while using the self-draining bipolar plate. The study assessed various factors including voltage over-potential, the maximum power point, and continuous operation.

2. Self-draining bipolar plate fuel cells

2.1. Development of the self-draining bipolar plate

This paper is based on experimental studies conducted on a self-draining bipolar plate fuel cell. The concept of developing a self-draining bipolar plate arose from the challenges associated with flooding in conventional flow field systems, such as flow channel obstruction, which can lead to failure and increased concentration losses.

The bipolar plate under consideration features several conical passages, with the smaller diameter in contact with the MEA and the larger diameter exposed to the chamber through which hydrogen gas enters and exits. As the gas flows into the chamber, it passes through these conical apertures and then through the GDL to reach the platinum catalyst layer, where electrochemical reactions occur. This design promotes a uniform hydrogen concentration across the MEA, thereby reducing the likelihood of concentration losses.

The conical passages reduce the cross-sectional area of the flow, resulting in increased gas velocity at the GDL. Furthermore, the gas enters the chamber and moves through the conical passage both tangentially and axially, creating eddies within the passage. These eddies, along with the channel's slope, assist in expelling the trapped liquid water from the gas flow path, facilitating its removal from the chamber. An added advantage of this arrangement is that the increased gas velocity can push the gas deeper and more evenly across the MEA, enhancing gas utilization.

2.2. Description of the self-draining bipolar plate

The self-draining bipolar plate features a main body with an integrated chamber through which gases enter and partly exit. The rear of the main body connects to the cell's end plate, with a current collector positioned in between. At the front end, there is a rectangular slot designed to accommodate

the draining plate. To prevent gas leakage, O-ring grooves are provided at the rear of the main body for securing the O-rings. Additionally, two holes, each with a diameter of 2 mm, are located in the middle of two of the O-ring grooves to facilitate the flow of gas into and out of the chamber.

Figure 1A displays the draining plate, which has the larger cross-sectional face of the conical passage exposed to the chamber, while the smaller face contacts the MEA. Figure 1B depicts the assembly of the bipolar plate, which houses both the chamber and the draining plate. The draining plate measures 50 mm by 50 mm with a thickness of 2 mm. The conical passage has a larger diameter of 6.5 mm and a smaller diameter of 3 mm.

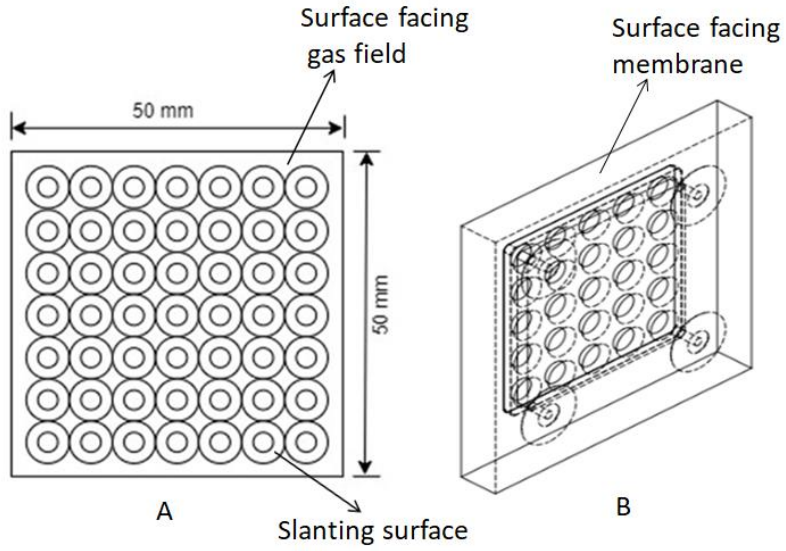

Figure 1. (A) Sketch showing the plate with a conical passage. (B) Bipolar plate assembly with the drain plate in position (circle with the bigger diameter, 6.5 mm: End exposed to the gas; circle with the smaller diameter, 3 mm: End exposed to the MEA. Thickness of the plate, 2 mm).

The chamber has a cross-section area of 46 mm × 46 mm and a height of 5 mm. The overall size of the bipolar plate is 75 mm × 75 mm × 10 mm.

3. Methodology

The objective of this study was to evaluate the performance of a low-temperature proton exchange membrane fuel cell (L-PEMFC) equipped with a self-draining bipolar plate and to assess its response to varying hydrogen flow rates and excess oxygen supplies. Additionally, the study aimed to investigate how the self-draining bipolar plate influences the fuel cell's performance at different humidification temperatures.

To further explore the performance dynamics, the fuel cell was operated continuously for 4.5 hours to observe fluctuations in the voltage and power under a given load. These experiments were conducted under both lower and higher catalyst loadings to determine whether reduced catalyst concentrations could be employed without significantly affecting the performance parameters.

3.1. Scheme of the experiment

In Scheme 1, experiments were conducted with three different hydrogen flow rates. For each flow rate, oxygen was supplied at varying volumes relative to the hydrogen flow rate: 50% (stoichiometric requirement with 0% excess oxygen), 75% (50% excess oxygen), 100% (100% excess oxygen), and 125% (150% excess oxygen). Voltage and power output values were recorded at 0.2-A intervals, beginning from no load until the fuel cell could no longer sustain the load, as indicated by a stable current. Current density values were calculated from the recorded current, and the voltage output was plotted against current density to generate a polarization curve. Similarly, power output was plotted against current density to produce a power versus current density curve.

The polarization curve was used to analyze voltage over-potential, while the power versus current density curve helped identify the maximum power point. The optimal hydrogen flow rate and excess oxygen supply were determined separately for both the higher and lower catalyst loadings, and these conditions were then applied to the experiments in Scheme 2.

In Scheme 2, experiments were conducted across a range of humidification temperatures from 60 to 100 ℃ in 10 ℃ increments, as well as under no humidification conditions. Voltage and power output data were utilized to generate both polarization curves and power curves. The polarization curve was analyzed to assess the voltage over-potential, while the power versus current density curve was employed to determine the maximum power point. On the basis of the power curve, the optimal humidification temperature within the specified range was identified for higher and lower catalyst loadings. These optimal conditions were subsequently used for the experiments in Scheme 3.

In Scheme 3, the fuel cell was operated continuously for approximately 5 hours to examine fluctuations in the voltage and power for both higher and lower catalyst loadings. The load (current) was maintained at the optimal value determined from Scheme 2, with the current density set to 88 mA/cm² for the higher catalyst loading and 80 mA/cm² for the lower catalyst loading.

Table 1. Scheme of the experiments.

Scheme 1 (for both the higher and lower catalyst loadings) for various hydrogen gas flow rates and excess oxygen supply Load: from OCV to maximum load-bearing capacity												
Hydrogen flow rate	80 ml/min				100 ml/min				120 ml/min			
Excess oxygen supply	0%	50%	100%	150%	0%	50%	100%	150%	0%	50%	100%	150%
Scheme 2 (for both the higher and lower catalyst loadings) for the best values of hydrogen flow rate and excess gas supply from Scheme 1 Load: from OCV to maximum load-bearing capacity												
Hydrogen humidification temperature (°C)	100	90	80	70	60	No humidification						
Hydrogen line temperature (°C)	110	100	90	80	70							
Oxygen humidification temperature (°C)	60	60	60	60	60	60						
Oxygen line temperature (°C)	70	70	70	70	70	70						
Scheme 3 (higher and lower catalyst loading) at the current density for the best humidification temperature from Scheme 2 Continuous operation for 4.5 hours												

3.2. Experimental set-up

To conduct the experiments outlined in Table 1, a fuel cell test station was utilized, which included two humidifiers—one for hydrogen gas and one for oxygen gas. The station was equipped with two Alison mass flow controllers, managed via a computer dashboard to ensure precise gas flow rates. The humidifiers were fitted with heating elements, which were also controlled via the dashboard, to regulate the humidification temperatures.

Gas was supplied to the fuel cell test station from a gas bank through a series of pipes, including a dedicated pipe for the nitrogen gas used for cell purging. Steel pipes were employed for the nitrogen and oxygen gases, while a copper pipe was used for hydrogen. A schematic diagram of the test station and the balance of the system is presented in Figure 2.

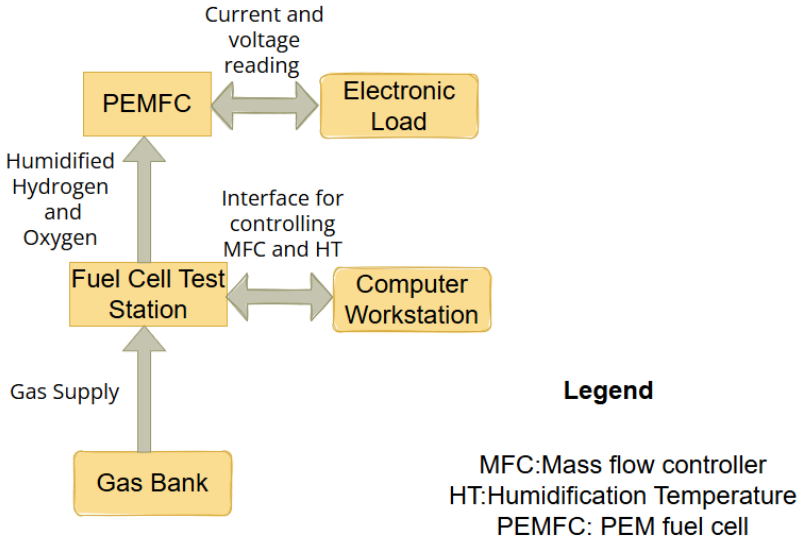

Figure 2. Schematic diagram of the fuel cell test station and the balance of the system.

3.3. Details of the experimental setup

Membrane electrode assembly: The MEA used in this study consisted of a Nafion 212 membrane, PTFE-treated carbon paper as the GDL, and platinum catalyst supported on carbon. Two different platinum catalyst loadings were employed to investigate whether lower catalyst loadings yielded performance parameters comparable with those obtained with higher catalyst loadings. For the MEA with the lower catalyst loading, the platinum loading was 0.2 mg/cm² on the anode side and 0.4 mg/cm² on the cathode side. In contrast, the higher catalyst loading featured 0.25 mg/cm² on the anode side and 0.5 mg/cm² on the cathode side. The active area of the MEA was 50 mm × 50 mm, with an overall membrane area of 75 mm × 75 mm, approximately matched to the area of the draining plate, which also measured 50 mm × 50 mm.

Fuel cell end plates: The end plates were constructed from steel and featured two recesses for the pneumatic gas connectors, which were used to supply and exhaust gases.

Current collector plates: Copper current collector plates are employed to gather electrons from the bipolar plate and are connected to the electronic load. The surface of each collector plate that contacts the end plate was coated with an electric insulation paint.

Electronic load: The electronic load system applied a load to the fuel cell. Leads from the electronic load were connected to the fuel cell's current collectors. The system included a display unit that showed the voltage developed by the fuel cell, the current load applied, and the power generated. In this study, voltage and power values were recorded at 0.2-A intervals until the saturation point was reached.

Line heaters: To prevent condensation of water vapor before it entered the fuel cell system, the humidified gas from the fuel cell work station was passed through a pipe equipped with a heater. This heater maintained the temperature of the gas above the humidification temperature, with the line temperature being regulated via the computer dashboard.

4. Results and discussion

The results covering voltage and power output were obtained from the electronic load system across a range of loads and operating conditions. These conditions featured varying hydrogen flow rates, excess oxygen supplies, hydrogen humidification temperatures, and continuous operation, with a specific focus on different platinum catalyst loadings.

The obtained results were analyzed to evaluate the effects of employing membranes with two distinct platinum catalyst loadings in combination with the self-draining bipolar plate.

4.1. Effect of higher and lower catalyst loading on the polarization curve and voltage over-potential

The voltage output values for various loads are plotted for hydrogen gas flow rates of 80, 100, and 120 ml/min hydrogen gas flow rates alongside excess oxygen supplies of 0, 50, 100, and 150%. This results in three distinct sets of polarization curves, as illustrated in Figure 3. Specifically, Figure 3A corresponds to an 80 ml/min hydrogen flow rate, while Figure 3B and Figure 3C represent the 100 ml/min and 120 ml/min flow rates, respectively.

A notable aspect of this study is the ability of the fuel cell equipped with a self-draining bipolar plate to handle loads significantly exceeding 120 mA/cm^2. The design of the gas passage minimizes the likelihood of water obstructing the gas during dynamic gas movement. Additionally, the conical shape of the passages is expected to enhance the gas's velocity toward the MEA, facilitating the transport of both gas and moisture to the catalyst—GDL interface.

Figure 3A displays distinct voltage values for various levels of excess oxygen supply at a hydrogen flow rate of 80 ml/min. Notably, higher excess oxygen (150%) yields increased voltage values, particularly at elevated loads; however, the voltage outputs show minimal variation between the two catalyst loadings. At higher hydrogen flow rates (100 ml/min in Figure 3B and 120 ml/min in Figure 3C), the polarization curves tend to converge, especially at 120 ml/min (Figure 3C). This convergence suggests that the increased gas velocity through the narrower conical passages enhances the likelihood of hydrogen molecules finding suitable reaction sites, leading to similar voltage outputs, particularly with a higher excess oxygen supply.

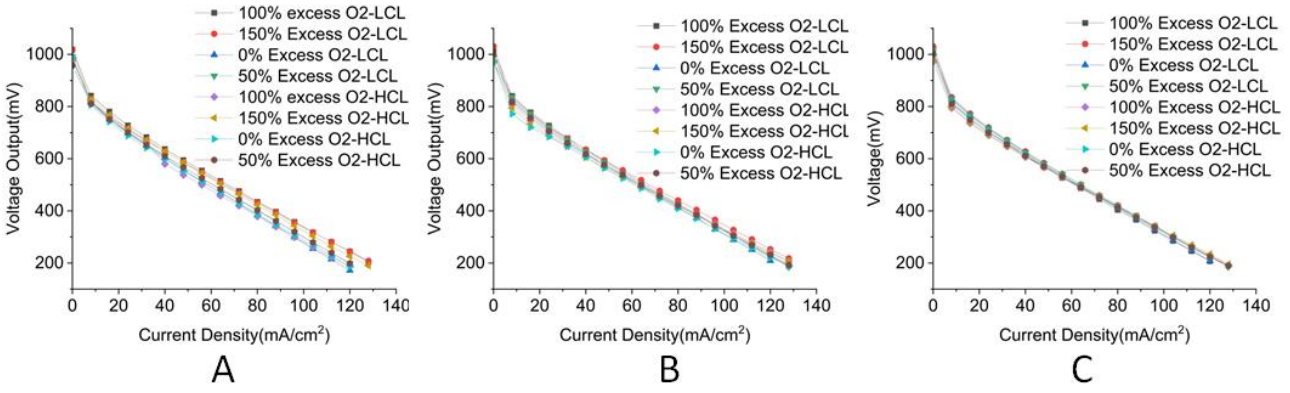

Figure 3. Polarization curves for different excess oxygen flow rates, and higher and lower catalyst loadings: (A) 80 ml/min H_2 flow rate; (B) 100 ml/min H_2 flow rate; (C) 120 ml/min H_2 flow rate. LCL, lower catalyst loading; HCL, higher catalyst loading; 100% Excess O_2, oxygen supply twice that of the stoichiometric oxygen requirement (SOR); 150% Excess O_2, oxygen supply one and half times the SOR; 50% excess O_2, 50% more than the SOR; 0% Excess O_2, equal to the SOR.

Furthermore, absence of concentration losses is indicated by the curves, as the gas directly contacts the MEA rather than travelling through flow channels, ensuring that no part of the MEA is deprived of fuel gas. Figure 3C notably shows that most curves converge across the entire range of current densities. This observation implies that at a hydrogen flow rate of 120 ml/min, it may be feasible to operate with lower catalyst loadings, potentially reducing the cost of the MEA. This hypothesis will be further evaluated through an analysis of various losses and load-bearing capacities.

Table 2. Voltage over-potential (LCL, lower catalyst loading; HCL, higher catalyst loading).

	Activation loss			Ohmic loss			Concentration loss			Ohmic loss/current density		
	Hydrogen flow rate (ml/min)			Hydrogen flow rate (ml/min)			Hydrogen flow rate (ml/min)			Hydrogen flow rate (ml/min)		
	100	120	80	100	120	80	100	120	80	100	120	80
100% Excess O2-LCL	463	567	504	360	238	311	0	0	0	5	4.8	4.8
150% Excess O2-LCL	475	650	458	338	189	261	0	0	0	4.9	4.9	4.7
0% Excess O2-LCL	423	597	476	368	201	341	0	0	0	5	5	5.3
50% Excess O2-LCL	427	561	424	357	272	369	0	0	0	5	4.9	5
100% Excess O2-HCL	437	444	396	326	337	390	0	0	0	4.5	4.7	4.9
150% Excess O2-HCL	485	490	397	284	297	396	0	0	0	4.4	4.6	5
0% Excess O2-HCL	484	544	435	298	255	369	0	0	0	4.7	4.6	5
50% Excess O2-HCL	501	510	390	306	292	368	0	0	0	4.8	4.6	5

Table 2 presents data on voltage over-potential for various hydrogen flow rates and two different catalyst loadings. It also includes the ratio of ohmic loss to current density, which serves as an indicator of the fuel cells' stability under load. A higher ratio signifies lower stability, while a lower ratio reflects improved stability. Activation loss, a critical factor influencing the fuel cells'

performance, significantly reduces voltage output when elevated. Table 2 indicates that activation losses are highest at a hydrogen flow rate of 120 ml/min, irrespective of the excess oxygen supply or catalyst loading.

The fuel cell examined in this study is of the L-PEMFC type and lacks a heating mechanism. As a result, higher hydrogen flow rates led to a decrease in the operating temperature due to the heat being carried away by the gas. Additionally, the conical shape of the gas passage may have further contributed to cooling effects, negatively influencing the chemical kinetics and leading to increased activation losses.

When we compare activation losses for higher and lower catalyst loadings, the differences are minimal; most values are closely aligned. Generally, higher platinum loading enhances fuel cell kinetics. However, a 20% reduction in platinum loading on the anode side does not yield a significant change in activation loss values, likely due to the specialized flow field design that improves gas distribution in terms of both its spread and penetration.

Ohmic loss plays a more pivotal role in overall fuel cell efficiency. Even with lower activation losses, a higher ohmic loss slope can diminish the overall efficiency. The experiments demonstrate that ohmic losses at various current densities are lower for a hydrogen flow rate of 120 ml/min, contrasting with higher activation losses, as noted in Table 2. This observation explains why polarization curves converge at extreme current density loads, except at an 80 ml/min hydrogen flow rate, where the steeper slope of ohmic loss to current density results in divergent polarization curves. Furthermore, the steeper slope associated with higher catalyst loading contributes to the increased divergence of the curves, as illustrated in Figure 3.

4.2. Effect of higher and lower catalyst loading on power output and the maximum power point

Figure 4 displays the power output across different loads, excess oxygen supplies, and hydrogen flow rates. Specifically, for a hydrogen flow rate of 80 ml/min, the power output is shown in Figure 4A; that for 100 ml/min is depicted in Figure 4B and that for 120 ml/min is represented in Figure 4C.

At lower current densities, the power output values for various excess oxygen supplies remain within a narrow range for substantial load values. For a hydrogen flow rate of 120 ml/min, the difference between the maximum and minimum power output values ranges from 0 to 28 mW across a current density range of 0 to 72 mA/cm². In comparison, for a hydrogen flow rate of 100 ml/min, this variation occurs within a current density range of 0 to 32 mA/cm², and for 80 ml/min, the range is 0 to 24 mA/cm². This suggests that to achieve comparable power outputs, the optimal hydrogen flow rate is 120 ml/min, although this is limited to part-load operation. At higher loads, power output becomes increasingly dependent on the excess oxygen supply and hydrogen flow rate. The efficiency of a fuel cell is determined by the maximum power achievable under specific conditions. Applications with lower power requirements typically experience varying loads, predominantly operating at partial load. As demonstrated in Figure 4, the fuel cell performs optimally at partial loads. Ideally, the maximum power point indicates the best operating condition. It is important to examine the range of load values at which the maximum power point occurs for both lower and higher catalyst loadings under different excess oxygen supplies. The data indicate that hydrogen flow rates of 100 ml/min and 120 ml/min are optimal for performance.

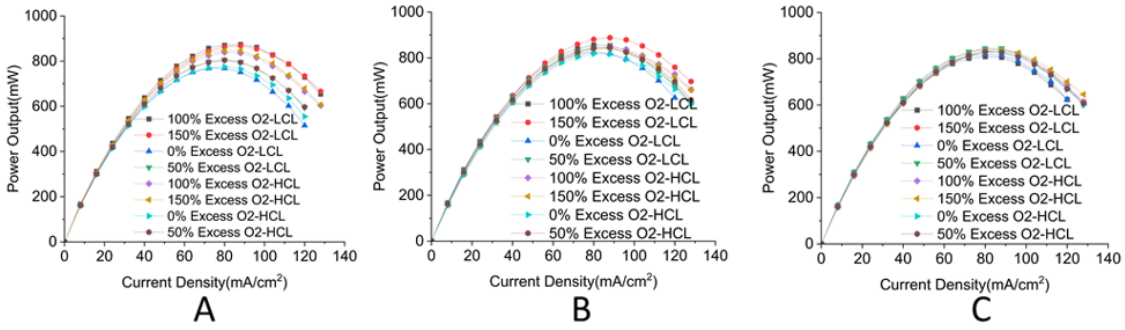

Figure 4. Power curves for different excess oxygen flow rates, and higher and lower catalyst loadings: (A) 80 ml/min H_2 flow rate; (B) 100 ml/min H_2 flow rate; (C) 120 ml/min H_2 flow rate. LCL, lower catalyst loading; HCL, higher catalyst loading; 100% Excess O_2, oxygen supply twice that of the stoichiometric oxygen requirement (SOR); 150% Excess O_2, oxygen supply one and half times the SOR; 50% Excess O_2, 50% more than the SOR; 0% Excess O_2, equal to the SOR.

The hydrogen flow rate of 120 ml/min provides a broader load range compared with 80 ml/min in all scenarios, including both maximum power output and at 5% and 10% below the maximum power output as can be seen in Table 3, regardless of the excess oxygen supply or platinum catalyst loading. Across the entire range of excess oxygen supplies, there is no significant difference in load range between higher and lower catalyst loadings.

The analysis concludes that the self-draining bipolar plate inherently accommodates a wide range of load variations under the part-load regime, allowing for a reduction in maximum power output of 5–10. The decision to accept a 5% or 10% reduction in maximum power output should be based on a trade-off between the reduction in power and the variability in current density and voltage output ranges.

Table 3. Current density range for maximum power value and 5% or 10% lower than the maximum power output.

Hydrogen flow rate (ml/min)	Maximum values LCL (mA/cm^2)	5% lower power LCL (mA/cm^2)	10% lower power LCL (mA/cm^2)	Maximum values HCL (mA/cm^2)	5% lower power HCL (mA/cm^2)	10% lower power HCL (mA/cm^2)
80	72–88	64–104	56–112	80–88	64–96	56–104
100	80–88	64–104	56–112	80–88	64–104	56–112
120	80–88	64–96	56–104	80–88	64–104	56–112

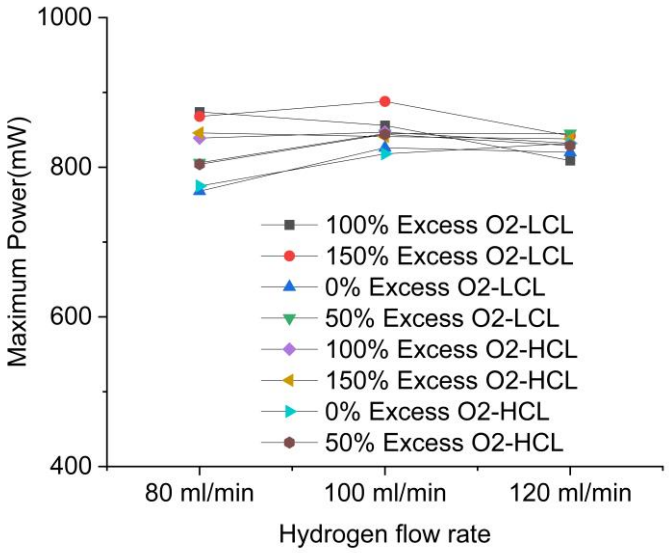

Figure 5. Maximum power point and maximum power.

Figure 5 displays the maximum power point (MPP) for various hydrogen flow rates and excess oxygen supplies. All MPPs fall within the load range of 80–88 mA/cm², indicating that the fuel cell operates optimally at the MPP when the load is maintained within this range, regardless of the excess oxygen supply or hydrogen flow rate. The maximum power output shows considerable variation with excess oxygen supply for a hydrogen flow rate of 80 ml/min. In contrast, the variation is somewhat smaller at 100 ml/min, while the values converge at 120 ml/min.

While it is commonly believed that increasing the amount of platinum catalyst in the MEA enhances performance, the findings of this study suggest otherwise. Two key factors must be considered to explain the observed decrease in maximum power with the higher catalyst loading. First, the self-draining bipolar plate used in this study differs from traditional serpentine designs. Its conical passages lead to the formation of eddies within the cavities, which affect the gas flow patterns, including the distribution and depth, potentially causing fluctuations in performance.

Secondly, the 20% variation in catalyst loading is relatively modest and insufficient to produce significant changes in the performance parameters. Moreover, the self-draining design of the bipolar plate effectively facilitates the removal of water accumulated in the conical passages, primarily due to the configuration of the passages and gas movement. However, the temporary presence of water during operation with increased catalyst loading may have slightly reduced the performance.

4.3. Comparison of the effect of humidification temperature on the performance of PEMFCs

The temperature for hydrogen gas humidification varied between 60 and 100 ℃, while the oxygen humidification temperature was consistently maintained at 60 ℃. Additionally, experiments were conducted under conditions with no humidification (0 ℃). These tests were performed separately for both lower and higher catalyst loadings, utilizing the self-draining bipolar plate in the fuel cell. The resulting polarization curves are shown in Figure 6.

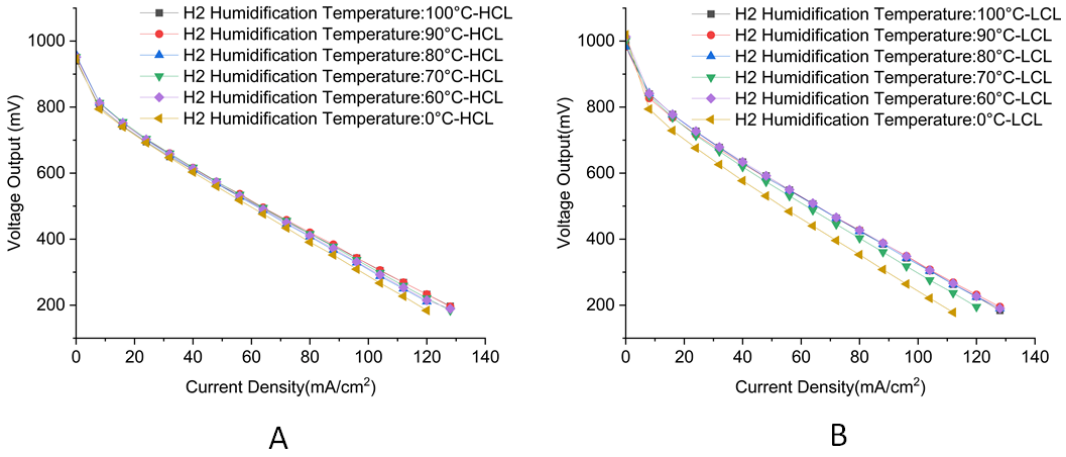

Figure 6. Polarization curves for different humidification temperatures. (A) Higher catalyst loading; (B) lower catalyst loading (0 °C: no humidification) with 100 ml/min hydrogen and 150% excess oxygen supply.

As anticipated, under conditions of no humidification, the polarization curves are lower for both the higher and lower catalyst loadings. The load-bearing capacity, defined as the maximum current density the fuel cell can support, is slightly improved with the higher catalyst loading compared with lower catalyst loading. Specifically, for the higher catalyst loading, the load-bearing capacity ranges from 120 to 130 mA/cm², while for lower catalyst loading, it ranges from 110 to 130 mA/cm².

Table 4. Voltage over-potential for different humidification temperatures.

	Humidification temperature (°C) Voltage over-potential (mV)	100	90	80	70	60	No humidification
Lower catalyst loading	Ohmic loss	365	353	357	343	360	399
	Activation loss	440	435	436	463	463	442
Higher catalyst loading	Ohmic loss	376	378	358	391	342	419
	Activation loss	371	380	389	377	421	428

The voltage over-potential extracted from the polarization curve is presented in Table 4. Both activation losses and ohmic losses significantly influence the performance of a PEMFC. While activation losses reduce the polarization curve, the slope of the ohmic loss decides the overall loss of the fuel cell. As shown in Table 4, activation losses are higher for lower catalyst loadings compared with higher catalyst loadings, whereas ohmic losses increase with higher catalyst loadings. The overall losses are minimized within the humidification temperature range of 80–90 ℃. Notably, concentration losses are absent, as the hydrogen gas supplied to the anode flows uniformly through all conical passages, ensuring that no part of the MEA is deprived of hydrogen. At a humidification temperature of 100 ℃, activation losses are minimized due to enhanced chemical kinetics at elevated temperatures. In contrast, lower humidification temperatures and conditions without humidification impede the reaction, leading to increased activation losses.

On comparing the load-bearing capacity of conventional flow field bipolar plate with self-draining bipolar plate, in the worst case scenario, the values are 100 and 130 mA/cm^2, respectively,

for conventional and self-draining bipolar plates. This amounts to an improvement of about 30% in load-bearing capacity.

4.4. Comparison of the effect of humidification temperature on MPP

The power output of a PEMFC equipped with a self-draining bipolar plate is illustrated in Figure 7, which compares different humidification temperatures and catalyst loadings across various loads. Figure 7A,B presents data for the higher and lower catalyst loadings. For both catalyst loadings, the power output is lowest under no humidification conditions compared with all other humidification temperatures. However, for the higher catalyst loading, power output values remain relatively consistent up to a load of 40 mA/cm², while for the lower catalyst loading, the power output begins to diverge at a low load of 10 mA/cm². Maintaining a high power output across varying humidification temperatures is advantageous; higher catalyst loading is preferable. Specifically, for the higher catalyst loading, the power output at the MPP is 836, 841, 817, 832, 823, and 783 mW/cm² for humidification temperatures of 100, 90, 80, 70, 60 °C, and zero humidification, respectively. For the lower catalyst loading, the corresponding power outputs are 853, 855, 848, 806, 856, and 713 mW/cm², respectively.

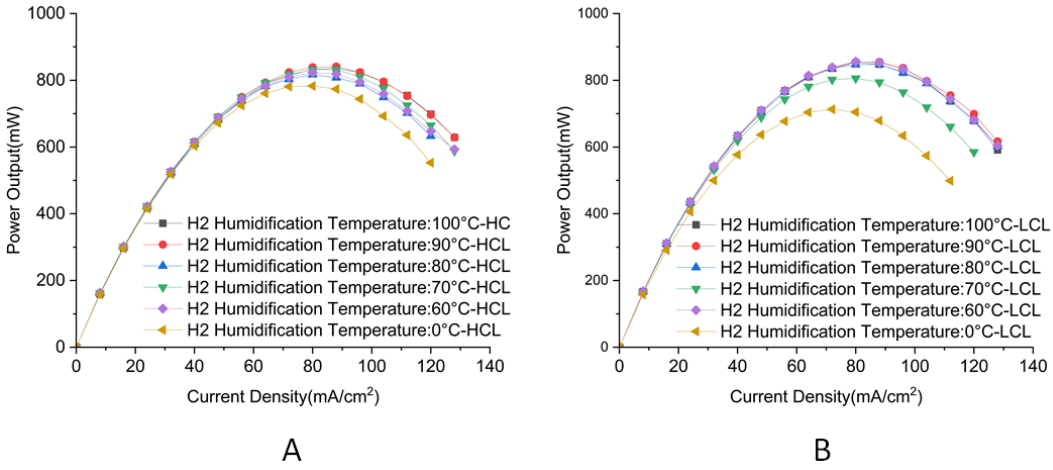

Figure 7. Power output for different humidification temperatures and the higher and lower catalyst loading for the fuel cell with a self-draining bipolar plate.

For a 5% reduction in maximum power, the higher catalyst loading results in a current density range of 64–104 mA/cm², whereas the lower catalyst loading yields a range of 56–96 mA/cm². This suggests that there is no significant advantage associated with either type of catalyst loading. Furthermore, the highest maximum power for both the higher and lower catalyst loadings is achieved at a humidification temperature of 90 °C. Additionally, a 5% decrease in maximum power would broaden the operating current density range, which remains consistent for both catalyst loadings at 72–96 mA/cm².

4.5. The fuel cell's behavior during continuous operation for the higher and lower catalysts loading with a self-draining bipolar plate

We conducted continuous operation for four and a half hours for both the higher and lower catalyst loadings, utilizing the optimal hydrogen flow rate, oxygen supply, humidification temperature, and MPP. The resulting voltage and power values plotted against time are shown in Figure 8. Figure 8A displays the voltage output, while Figure 8B depicts the power output.

Figure 8 reveals that the output versus time graphs exhibit three distinct regions: A region of rapid change, an unstable region, and a stabilization region. These patterns are evident in both the voltage and power graphs, regardless of the catalyst loading.

In the initial region, there is a sharp increase from the initial voltage and power values to their maximum levels. This rapid change occurs because the system cannot immediately respond to the transition from open-circuit voltage to the desired current density. As a result, the initial voltage and power values are low but rise rapidly to their peak, often exceeding the designed value for the given load.

Once the maximum values are reached, both voltage and power gradually decrease, approaching stable values. Approximately one and a half hours after the load is applied, the fuel cell stabilizes, producing relatively steady voltage and power, thus establishing a stable region with appropriate values for the given load. Minor variations within the stable region can be attributed to periodic water drainage from the conical passages.

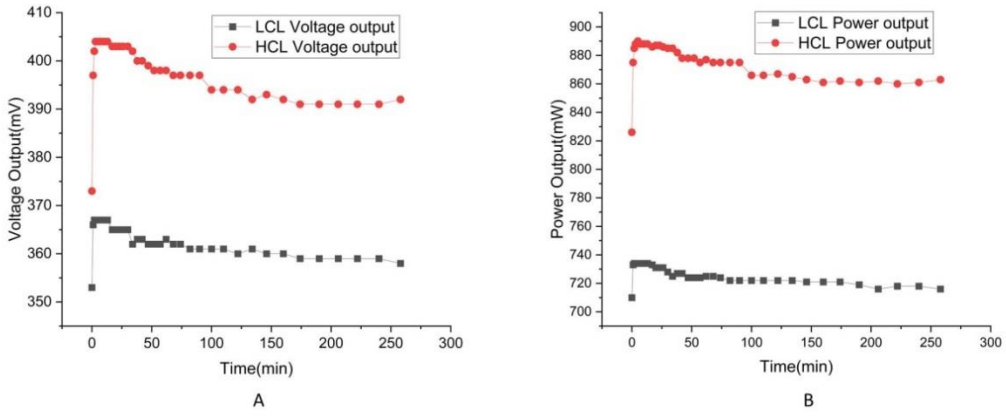

Figure 8. Voltage output and power output with continuous operation for the lower and higher catalyst loading: (A) voltage output; (B) power output. Operating conditions for the lower catalyst loading: Hydrogen flow rate, 100 ml/min; excess oxygen supply, 100%; H_2 humidification temperature, 90; H_2 line temperature, 100; O_2 humidification temperature, 60; O_2 line temperature, 70; current density, 80 mA/cm^2. Operating condition for the higher catalyst loading: Hydrogen flow rate, 100 ml/min; excess oxygen supply, 50%; H_2 humidification temperature, 90; H_2 line temperature, 100; O_2 humidification temperature, 60; O_2 line temperature, 70; current density, 88 mA/cm^2.

5. Conclusions

Based on the discussions in the previous section, the following conclusions can be drawn.

The fuel cell equipped with a self-draining bipolar plate is capable of supporting loads exceeding 120 mA/cm², representing approximately a 30% increase in load capacity compared with conventional flow field-based systems

On comparing the ability of the fuel cell to perform at two levels of catalyst concentration with a difference of about 20%, operating with self-draining bipolar plates, it was found that even at lower concentration levels, the fuel cell could produce comparable results, thereby reducing both the initial and operating costs.

The fuel cell was operated with varying amounts of hydrogen gas and it was found that lower hydrogen flow rates result in varying voltage values, depending on the excess oxygen supply; however, these values are nearly identical for both catalyst loadings, namely 0.20 mg/cm^2 (anode) with 0.40 mg/cm^2 (cathode, and 0.25 mg/cm^2 (anode) with 0.50 mg/cm^2 (cathode). Furthermore, at higher hydrogen flow rates, no significant differences were observed in the voltage.

On comparing the power output at different loads, it was found that at higher loads, the power output is influenced by excess oxygen supply, whereas at lower (partial) loads, power output is independent of the excess oxygen supply. The load range for this condition is widest for 120 ml/min.

Further, it was observed that the maximum power is achieved at partial loads, and the MPP is achieved when the load is maintained between 80 and 88 mA/cm². The fuel cell can operate over a broader range with a 5–10% reduction in power at maximum power output across all excess oxygen conditions.

On experimenting with different humidification temperatures, the highest power output was obtained at 90 °C for both the higher and lower catalyst loadings. However, for the higher catalyst loading, power output remains consistent up to a load of 40 mA/cm², while for the lower catalyst loading, it remains steady up to 10 mA/cm². Further, a 5% reduction in power at the maximum power point increases the load capacity by the same amount for both catalyst loadings.

Other observations are (i) the self-draining design helps create a cooling effect, which lowers the fuel cell temperature but also increases activation losses; (ii) concentration losses are negligible under all operating conditions; and (iii) continuous operation of the fuel cell under optimal conditions shows similar behavior for both catalyst loadings, with three distinct regions identified.

Use of AI tools declaration

In the preparation of this document, the authors have not utilized any AI tool.

Acknowledgment

This work was supported by an All India Council for Technical Education (AICTE) grant funded by the Government of India (No.8-168/FDC/RPS (Rural)/POLICY-1/2021-22). The authors profusely thank the AICTE for the support provided by the agency.

Conflict of interest

The authors have no conflicts of interest to disclose.

Author contributions

Sudesh Bekal: Concieved the idea, designed the methodology, carried out the experiment, and wrote the paper; Shripad T Revankar: Supervised the project, reviewed the paper.

References

1. Li H, Tang Y, Wang Z, et al. (2008) A review of water flooding issues in the proton exchange membrane fuel cell. *J Power Sources* 178: 103–117. https://doi.org/10.1016/j.jpowsour.2007.12.068.
2. Bao C, Ouyang M, Yi B (2006) Modeling and control of air stream and hydrogen flow with recirculation in a PEM fuel cell system—I. Control-oriented modeling. *Int J Hydrogen Energy* 31: 1879–1896. https://doi.org/10.1016/j.ijhydene.2006.02.031
3. Natarajan D, Nguyen TV (2003) Three-dimensional effects of liquid water flooding in the cathode of a PEM fuel cell. *J Power Sources* 115: 66–80. https://doi.org/10.1016/S0378-7753(02)00624-9S
4. Karthikeyan M, Muthukumar M, Karthikeyan P, et al. (2019) Optimization of active area of proton exchange membrane fuel cell with better water management. *J Ceram Proc Res* 20: 490–498. https://doi.org/10.36410/jcpr.2019.20.5.490.
5. Palaniswamy K, Marappan M, Rajendran JV (2016) Influence of porous carbon inserts on scaling up studies for performance enhancement on PEMFC. *Int J Hydrogen Energy* 41: 2867–2874. https://doi.org/10.1016/j.ijhydene.2015.10.148
6. Desai AN, Mohanty S, Ramadesigan V, et al. (2022) Investigating the water flooding effects on the performance of low-temperature proton exchange membrane fuel cell. *Proceedings of WHEC 2022—23rd World Hydrogen Energy Conference: Bridging Continents by H2*, 772–774. Available from: https://www.proceedings.com/content/065/065069webtoc.pdf.
7. Bozorgnezhad A, Shams M, Ahmadi G, et al. (2015) The experimental study of water accumulation in PEMFC cathode. *ASME/JSME/KSME 2015 Joint Fluids Engineering Conference, AJKFluids 2015*. https://doi.org/10.1115/AJKFluids2015-22299
8. Liao P, Xu S, Ming P, et al. (2021) The effects of anode serpentine flow field structure and humidity on performance of PEMFCs. *ECS Trans* 104: 295–305. https://doi.org/10.1149/10408.0295ecst
9. Shen J, Xu L, Chang H, et al. (2020) Partial flooding and its effect on the performance of a proton exchange membrane fuel cell. *Energy Convers Manage*, 207. https://doi.org/10.1016/j.enconman.2020.112537
10. Aslam RM, Ingham DB, Ismail MS, et al (2018) Simultaneous direct visualisation of liquid water in the cathode and anode serpentine flow channels of proton exchange membrane (PEM) fuel cells. *J Energy Inst* 91: 1057–1070. https://doi.org/10.1016/j.joei.2017.07.003

11. Kim K, Kim J, Choi H, et al. (2023) Pre-diagnosis of flooding and drying in proton exchange membrane fuel cells by bagging ensemble deep learning models using long short-term memory and convolutional neural networks. *Energy*, 26. https://doi.org/10.1016/j.energy.2022.126441
12. Cho JIS, Neville TP, Trogadas P, et al. (2018) Capillaries for water management in polymer electrolyte membrane fuel cells. *Int J Hydrogen Energy* 43: 21949–21958. https://doi.org/10.1016/j.ijhydene.2018.10.030
13. Pei H, Song S, Wang Z, et al. (2022) Effect of inner dehumidification technique on the performance of a dead-ended proton exchange membrane fuel cell stack. *Int J Energy Res* 46: 6436–6443. https://doi.org/10.1002/er.7580
14. Sanchez DG, Ruiu T, Biswas I, et al. (2014) Effect of the inlet gas humidification on PEMFC behavior and current density distribution. *ECS Trans* 64: 603–617. https://doi.org/10.1149/06403.0603ecst
15. Xu X, Li K, Liao Z, et al. (2022) Closed-loop water management methodology for PEM fuel cell system based on impedance information feedback. *Energies* 15: 7561. https://doi.org/10.3390/en15207561
16. Chen X, Xu J, Liu Q, et al. (2020) Active disturbance rejection control strategy applied to cathode humidity control in PEMFC system. *Energy Convers Manage*, 224. https://doi.org/10.1016/j.enconman.2020.113389
17. Kang S (2015) Quasi-three dimensional dynamic modeling of a proton exchange membrane fuel cell with consideration of two-phase water transport through a gas diffusion layer. *Energy* 90: 1388–1400. https://doi.org/10.1016/j.energy.2015.06.076
18. Natarajan D, Van Nguyen T (2001) A two-dimensional, two-phase, multicomponent, transient model for the cathode of a proton exchange membrane fuel cell using conventional gas distributors. *J Electrochem Soc* 148: a1324–a1335. https://doi.org/10.1149/1.1415032
19. Shimpalee S, Greenway S, Van Zee JW (2006) The impact of channel path length on PEMFC flow-field design. *J Power Sources* 160: 398–406. https://doi.org/10.1016/j.jpowsour.2006.01.099
20. Springer TE, Zowodzinski TA, Gottesfeld S (1991) Polymer electrolyte fuel cell model. *J Electrochem Soc* 138: 2334–2342. https://doi.org/10.1149/1.2085971
21. Cheng W, Yu Y, Tu Z (2019) Study on removal time of droplets in the electrolyte of hydrogen-oxygen fuel cell. *J Wuhan Univ Technol (Trans Sci Eng)* 43: 652–656. https://doi.org/10.3963/j.issn.2095-3844.2019.04.015.
22. Li Y, Zhou Q, Zhang X (2014) Numerical analysis of steady state self-humidification performance of PEMFC. *CIESC J* 65: 1893–1899. https://doi.org/10.3969/j.issn.0438-1157.2014.05.048

AIMS Press